Citation: Anssi Pelkonen, Ropafadzo Mzezewa, Lassi Sukki, Tomi Ryynänen, Joose Kreutzer, Tanja Hyvärinen, Andrey Vinogradov, Laura Aarnos, Jukka Lekkala, Pasi Kallio, Susanna Narkilahti. (2020) A modular brain-on-a-chip for modelling epileptic seizures with functionally connected human neuronal networks. Biosensors and Bioelectronics Volume 168, 15 November 2020. https://doi.org/10.1016/j.bios.2020.112553

This is the final version accepted for the publication

A modular brain-on-a-chip for modelling epileptic seizures with functionally connected human neuronal networks

Anssi Pelkonen[1], Ropafadzo Mzezewa[1], Lassi Sukki[2], Tomi Ryynänen[2], Joose Kreutzer[2], Tanja Hyvärinen[1], Andrey Vinogradov[1], Laura Aarnos[1], Jukka Lekkala[2], Pasi Kallio[2] and Susanna Narkilahti[1]*

1 NeuroGroup, Faculty of Medicine and Health Technology, Tampere University, Tampere, Finland

2 Micro- and Nanosystems Research Group, Faculty of Medicine and Health Technology, Tampere University, Tampere, Finland

*Corresponding author

E-mail: susanna.narkilahti@tuni.fi

Tel.: +358 40 708 5113

ABSTRACT

Epilepsies are a group of neurological disorders characterised by recurrent epileptic seizures. Seizures, defined as abnormal transient discharges of neuronal activity, can affect the entire brain circuitry or remain more focal in the specific brain regions and neuronal networks. Human pluripotent stem cell (hPSC)-derived neurons are a promising option for modelling epilepsies, but as such, they do not model groups of connected neuronal networks or focal seizures. Our solution is a Modular Platform for Epilepsy Modelling *In Vitro* (MEMO), a lab-on-chip device, in which three hPSC-derived networks are separated by a novel microfluidic cell culture device that allows controlled network-to-network axonal connections through microtunnels. In this study, we show that the neuronal networks formed a functional circuitry that was successfully cultured in MEMO for up to 98 days. The spontaneous neuronal network activities were monitored with an integrated custom-made microelectrode array (MEA). The networks developed spontaneous burst activity that was synchronous both within and between the axonally connected networks, i.e. mimicking both local and circuitry functionality of the brain. A convulsant, kainic acid, increased bursts only in the specifically treated networks. The activity reduction by an anticonvulsant, phenytoin, was also localised to treated networks. Therefore, modelling focal seizures in human neuronal networks is now possible with the developed chip.

KEYWORDS

Epilepsy, functional circuitry, human stem cell derived neurons, in vitro disease modelling, microfluidic device, microelectrode arrays

1. INTRODUCTION

Epilepsy is a multifactorial neurologic condition affecting over 50 million people worldwide (Fiest et al., 2017). It is a disease of neuronal networks, where epileptic seizures can affect only a few networks in a small brain area (focal seizures) or affect most circuitries of the whole brain (generalised seizures) (Centeno and Carmichael, 2014; Fisher et al., 2017). Epilepsy treatment is

problematic, as up to one-third of patients do not benefit from existing drugs (Golyala and Kwan, 2017). This reflects, in part, the challenges in epilepsy modelling, in which the commonly used animal models have partially failed to support the development of more effective therapies. Human-specific and genetically relevant *in vitro* epilepsy models can be created from neural cultures differentiated from human pluripotent stem cells (hPSCs), particularly those differentiated from human induced pluripotent stem cells (hiPSCs) of epilepsy patients (Du and Parent, 2015; Grainger et al., 2018). However, simple hPSC-derived neural cultures are not competent to represent interconnected neuronal networks or model focal seizures. Brain organoids can contain features of separately functioning neuronal networks (Lancaster et al., 2017; Grainger et al., 2018), but their sample repeatability is still suboptimal due to self-patterning during maturation (Brighi et al., 2020). Furthermore, there are no commercially available electrophysiological measurement systems that could take full benefit of the organoids' 3-dimensional structure as they so far have been recorded with commercial 2D MEAs (Trujillo et al., 2019). Therefore, more feasible methods are needed for modelling epilepsy and seizures in ensembles of human neuronal networks.

Microelectrode arrays (MEAs) can be used to measure the electrical activity of hPSC-derived neuronal networks and to distinguish seizure-like activity (Du and Parent, 2015; Grainger et al., 2018). However, MEA recordings can last several hours, especially in pharmacological experiments with several drugs and/or concentrations (Johnstone et al., 2010). This creates a need for reliable environment control in the cell culture wells attached on a MEA plate, which requires elaborate technical solutions. Nevertheless, even when the question of environment control is resolved, the standard MEA plates are designed to measure only a single isolated neuronal network *per se*.

In previous brain-on-a-chip designs, neuronal *in vitro* cultures have been divided into separate networks using microfluidic cell culture devices, in which the connections between different networks can be created by micrometre-scale tunnels (Taylor, A. M. et al., 2003; van de Wijdeven et al., 2019). The microfluidic devices are often composed of polydimethylsiloxane (PDMS), a transparent organosilicon that bonds with typical, solid MEA surface materials (Morin et al., 2006). However, for efficient monitoring of electrical activity in neuronal networks, the channel layout of the cell culture

device and the electrode layout of the MEA need to be compatible and the MEA-PDMS attachment perfect. The chip design also needs to support long-term cell culture because of the relatively slow functional development of hPSC-derived neuronal networks that can take several weeks or months (Halldorsson et al., 2015; Odawara et al., 2016; Shimba et al., 2019; Hyvarinen et al., 2019).

In this study, our aim is to prove the concept of a novel lab-on-chip device combining microfluidic and MEA technology for studying seizure-like activity in human neuronal networks: the Modular Platform for Epilepsy Modelling *In Vitro* (MEMO). We designed a three-compartment microfluidic device in a closed chain format, and a custom MEA that is fully compatible with the microfluidic device and with a commercially available headstage. We designed a specific gas supply chamber and a plastic lid to gain valid environment control. These modules (MEA, microfluidic device, gas supply system) can be independently assembled for different experimental setups, depending on the research question. The neuronal cell cultures in MEMO were maintained up to 98 days. MEMO allowed precise control over axonally-mediated integration of hPSC-derived cortical networks which formed a functional circuitry. Seizure-like activity was observed only in kainic acid (KA) treated networks and the effects of an anticonvulsant, phenytoin (PHT), were also localised to targeted networks.

2. MATERIALS AND METHODS

2.1. Custom MEA fabrication and characterisation

The MEMO concept is to monitor seizure-like activity of hPSC-derived neuronal networks with MEA technology in three separate but axonally connected compartments (Fig. 1a). The axonal connections are enabled by microtunnels between the compartments (Fig. S1). Two custom MEA layouts were designed to follow the basic concept (Fig. 1b,c). The first custom MEA version, has 24 circular (⌀ 30 µm) electrodes per compartment and eight rectangular (35 µm x 50 µm) electrodes under the microtunnels between adjacent compartments (custom MEA version 1, n = 11, Fig. 1b). In the second custom MEA version the microtunnel electrodes are positioned in front of the

microtunnels (custom MEA version 2, *n* = 10, Fig. 1c). In both versions, tunnel electrodes were designed so that the tracks did not run under the PMDS. Apart from the position and shape (circular, ⌀ 30 µm in version 2) of the microtunnel electrodes, the two MEA versions are equal in design. The custom MEA fabrication followed the process described earlier (Ryynänen et al., 2018). Briefly, the MEAs consist of 49 mm × 49 mm ×1 mm soda lime glass substrate and 300 nm Ti tracks with an additional 300 nm ion beam-assisted e-beam-deposited titanium nitride (IBAD TiN) coating on electrodes. 500 nm plasma enhanced chemical vapor deposited silicon nitride (PECVD SiN) was used as the insulator layer. The custom MEAs were compatible with a MEA2100 120-electrode headstage (Multi Channel Systems GmbH [MCS], Germany) in terms of physical dimensions and contact pad layout.

The impedances of the different electrode types were measured at 1 kHz frequency using the MEA-IT120 impedance testing device (MCS) from six custom MEAs before platform assembly and biological experiments.

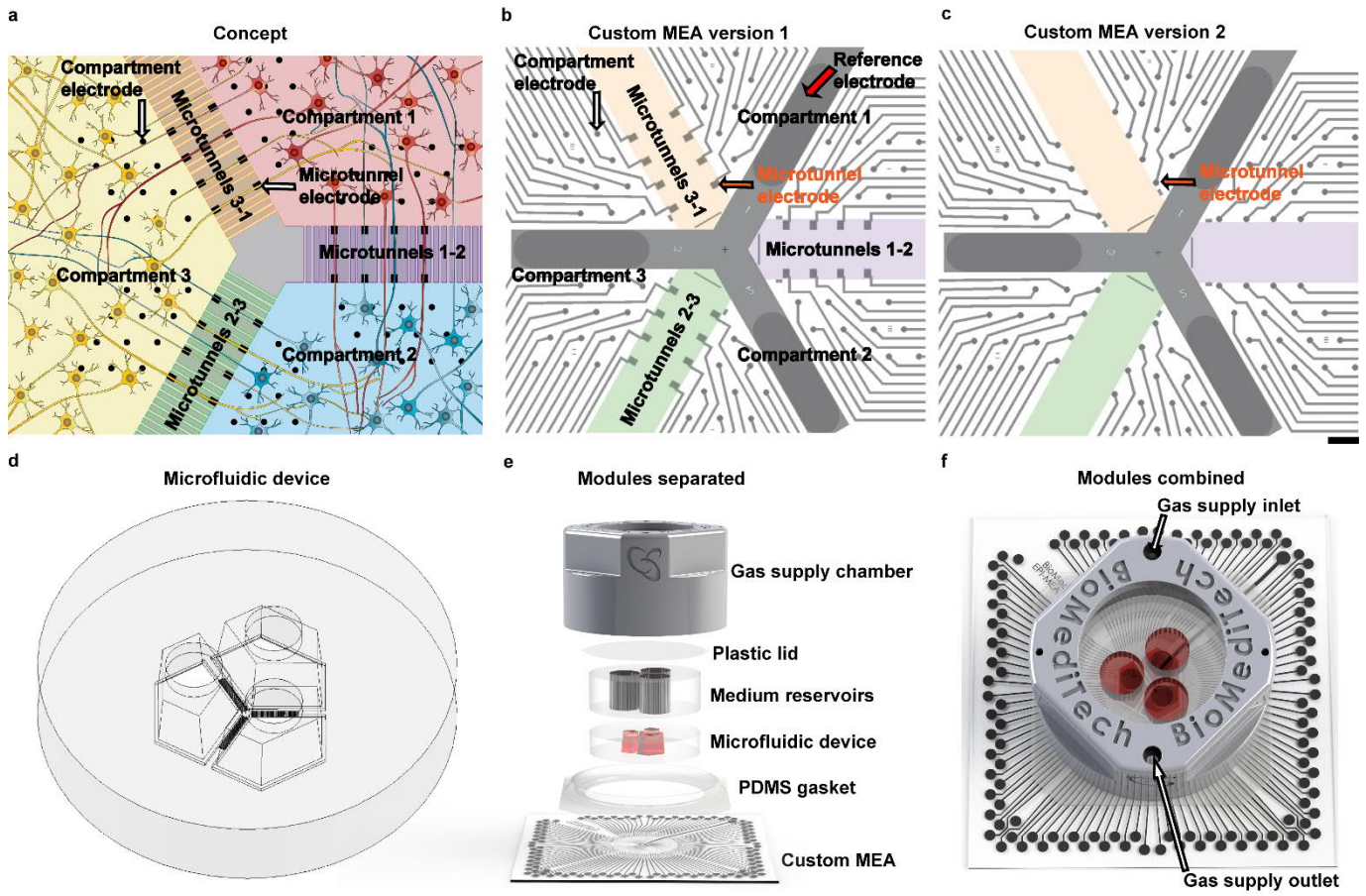

Fig.1. | Modular Platform for Epilepsy Modelling *In Vitro* (MEMO). a, Schematic representation of the MEMO concept, showing neuronal networks in separated compartments, connected through microtunnels (colour coded), and

surface embedded microelectrodes that measure neuronal network activity. **b**,**c,** Two custom-made MEA versions. The rectangular microtunnel electrodes in custom MEA version 1 are placed underneath the microtunnels (**b**), and the circular microtunnel electrodes in custom MEA version 2 are placed in front of the microtunnels (**c**). The intended position of the microtunnels is indicated with the colour coded areas in **b** and **c**. The reference electrode is also shown. The 200 µm scale bar in **c** also applies to **b**. **d,** Schematic representation of the microfluidic device showing the microtunnels and the compartments. **e,** 3D illustration showing all modules of the platform that are assembled in MEMO. **f,** Illustration of the modules combined.

2.2. Microfluidic device

MEMO contains a microfluidic device and a medium reservoir block (Fig. 1d,e). The microfluidic device was fabricated from PDMS using a modified version of micro- and millimetre-scale moulding technique as we previously described (Ristola et al., 2019). The mould consists of microscale features fabricated from SU-8 (SU-8 5 and SU-8 2150, micro resist technology GmbH) with photolithography (Taylor, A. M. et al., 2005) and macroscale inserts fabricated from UV-curable resin (Black v4, Formlabs Inc.) with stereolithography (SLA, Form 2, Formlabs Inc.) (Comina et al., 2014). The used resin provides a significant benefit of allowing PDMS to cure without additional treatments. The microfluidic device (⌀ 22 mm, height 4 mm) contains three compartments of pentagonal shape and 50 microtunnels between adjacent compartments (Fig. 1d). The microtunnels are 3.5 µm in height, 10 µm in width, 400 µm in length and 35 µm apart (edge-to-edge distance;Fig. S1). The medium reservoir block (⌀ 22 mm, height 7 mm, Fig. 1e,f) is placed on top of the microfluidic device to gain sufficient medium volume, 200 µl, per compartment. The block was also fabricated from PDMS by punching three holes to a PDMS block with a circular, ⌀ 6 mm punching tool.

2.3. Design and fabrication of gas supply system

Here, we utilised a similar technique for the gas supply system to prolong the measurements on MEA, as reported in our previous studies (Kreutzer et al., 2012; Metsälä et al., 2018). A PDMS gasket was used to seal the gas supply chamber to the MEA plate during the recordings (Fig. 1e,f). The gasket (inner ø 24 mm) was designed to fit the size of the cell culture device. The gas supply chamber was 3D printed with polypropylene-like material (RGD430, Object 30, Stratasys Ltd.). The

thin plastic lid (thickness 100 µm, ⌀ 24 mm) was cut with laser (Speedy 100, Trotec Laser GmbH) from polyester sheet.

2.4. Assembly and coating

The microfluidic device and the gasket were covalently bonded to the custom MEAs by treating all three parts with O_2 plasma (0.30 mbar, 50 W, 27 s; PICO plasma system, Diener Electronic GmbH + Co. KG). The microfluidic device was placed manually on the custom MEA under a microscope (SMZ1000, Nikon). Proper bonding between the MEA and the microfluidic device was ensured by placing a 145 g steel weight on top of the microfluidic device for ten minutes. The gasket was pressed onto the MEA using a circular plastic holder. The medium reservoir block was manually attached to the microfluidic device. The MEA and the compartments and microtunnels in the microfluidic device were coated immediately after assembly with 0.1 % polyethylenimine (PEI; Sigma-Aldrich) in borate buffer (1-1.5 h at room temperature). The excess PEI was washed three times with distilled and sterile H_2O, after which laminin (50 µg/ml, LN521, BioLamina) was added to the cell compartments and incubated overnight at +4 °C.

2.5. Maintenance of pH and osmolality

During MEA measurements longer than ten minutes, the pH and osmolality of the medium were maintained by covering the medium chambers with a sterile transparent plastic lid and by feeding the platform cell culture gas (5 % CO_2, 19 % O_2 and 76 % N_2) using the gas supply chamber. The gas flow rate was set to 5 ml/min using a Type 91 low bleed subminiature pressure regulator (Bellofram Corporation) and custom-made flow restrictor. The interface between the gasket and the gas supply chamber was sealed with a sterile silicone grease (Molykote, DuPont).

To validate the performance of the gas supply system, pH and osmolarity tests were performed. The pH measurements were performed with a SI400 pH metre (Sentron) in a volume of 70 µl immediately after taking the sample. The osmolality measurements were performed with an Osmomat 030 cryoscopic osmometer (Gonotec) in a volume of 50 µl directly after taking the sample. Measurements were performed at 80-95 days on MEMO (DOM) such that the control measurements

(MEMO kept in an incubator) were performed on the same week. The mediums were always changed a day before the first measurement.

2.6. Analysis of fluidic isolation between compartments

For analysis of fluidic isolation between the compartments, the microfluidic devices and glass coverslips (thickness 170 µm, ⌀ 30 mm) were bonded, combined with the medium reservoirs, coated and plated with cells as described above. Such devices were also used in certain imaging experiments with cells. In order to study diffusion of molecules between the compartments, fluorescein Na-salt (50 µM; MW 376.26 g/mol; F6377, Sigma-Aldrich) was added to Compartment 1. While the compartments themselves were filled with medium, the medium reservoirs of Compartments 1 and 3 were empty and Compartment 2 had a half-full medium reservoir (100 µl) to oppose diffusion from Compartment 1. The liquid's absorbance at 490 nm (proportional to the fluorescein concentration) in all three compartments was measured 1 h later with NanoDrop 2000 spectrophotometer (Thermo Fisher Scientific). Representative images of the fluorescein signal were attained with an IX51 microscope equipped with a DP30BW camera (both from Olympus Corporation).

2.7. Differentiation of cortical neurons

The human embryonic stem cell (hESC) line Regea 08/017 (Skottman, 2010) was used in this study. The Faculty of Medicine and Health Technology has the approval from the Finnish Medicines Agency (FIMEA) to perform research using human embryos (Dnro 1426/32/300/05). A supportive statement was also given by the regional ethics committee of Pirkanmaa Hospital District for the derivation, culture, and differentiation of hESCs (R05116). Prior to differentiation, hESCs were expanded in feeder-free culture on human recombinant laminin 521 (LN-521) and E8 medium (Thermo Fisher Scientific) as previously described (Hongisto et al., 2017). The cortical neural differentiation was performed as previously described (Hyvarinen et al., 2019). The experimental timeline is shown in Fig. 2.

Fig. 2. | **Timeline of experiments.** Human pluripotent stem cells (hPSCs) were pre-differentiated for 32 days before plating onto MEMO. The days *in vitro* (DIV) starting from the beginning of differentiation are shown above the line, and the days on MEMO (DOM) are shown below the line. Pharmacological experiments were performed after the emergence of synchronous bursts spanning all three compartments (DOM 55-62). The cells were characterised with immunocytochemistry after pharmacological experiments (DOM 62) and extended culture (DOM 98). Osmolality and pH measurements were performed on DOM 80-95.

2.8. MEA measurements

Neuronal activity in MEMO was recorded using a MEA2100 system (MCS). The temperature of the MEA headstage was kept at a steady +37 °C with a TC02 temperature controller (MCS). The medium chambers were covered with a sterile transparent plastic lid to prevent evaporation and contamination during measurements. The raw data were obtained at a sampling rate of 25 kHz. Standard 10-minute recordings were performed twice a week up to DOM 52 for monitoring the development of network activity. The platforms were imaged weekly using an Axio Observer.A1 inverted microscope equipped with an Axiocam 506 colour camera (both from Zeiss).

Seizure-like activity in MEMO was induced using KA (5 µM, K0250, Sigma-Aldrich) (Odawara et al., 2016) followed by an anticonvulsant, PHT, (50 µM, AB143201, Abcam) treatment (supplementary material, pharmacological experiments) (Chong et al., 2018). Pharmacological experiments were performed between DOM 55 and 62 and followed with standard recordings on DOM 66 until DOM 98 (Fig. 2).

2.9. Spike detection and MEA data analysis

For detecting neuronal spikes, the raw mcd-files were first converted to hdf5-file format using Multi Channel DataManager (MCS). Spike detection was performed on the hdf5-files using a previously

described method (Lieb et al., 2017; Mayer et al., 2018) embedded in an in-house made MATLAB (MathWorks) script.

Further MEA data analysis was performed in R (The R Foundation for Statistical Computing). Bursts were identified from the spike timestamps with logISI algorithm (Pasquale et al., 2010) with additional modifications (Hyvarinen et al., 2019)see supplementary material, MEA data analysis).

2.10. Immunocytochemistry and imaging

At the end of the biological experiments, immunocytochemistry was performed on the cells in selected microfluidic devices, either on custom MEAs or glass coverslips as described earlier (Lappalainen et al., 2010) with minor modifications (supplementary material, immunocytochemistry and imaging). The following primary antibodies were used: monoclonal mouse anti-β-tubulin III ([TUBB3] 1:50, T8660, Sigma-Aldrich), chicken polyclonal anti-TUBB3 (1:50, ab107216, Abcam) and polyclonal chicken anti-neurofilament protein H ([NF-H] 1:50, A00136, GenScript) for axons; polyclonal rabbit anti-microtubule-associated protein 2 ([MAP-2] 1:50; AB5622, Millipore) and chicken polyclonal anti-MAP-2 (1:50, NB300-213, Novus Biologicals) for dendrites; polyclonal chicken anti-glial fibrillary acidic protein ([GFAP] 1:4000, ab4674, Abcam) for astrocytes; rabbit monoclonal anti-synaptophysin ([SYP] 1:200, ab32127, Abcam) for presynaptic terminals; mouse monoclonal anti-postsynaptic density protein 95 ([PSD95] 1:50, ab2723, Abcam) for postsynaptic terminals; rabbit polyclonal anti-vesicular glutamate transporter 1 ([VGLUT1] 1:50, 135303, Synaptic Systems) for excitatory neurons; and mouse monoclonal anti-glutamic acid decarboxylase 67 kDa form ([GAD67] 1:50, MAB5406, Millipore) for inhibitory neurons (see supplementary material, immunocytochemistry and imaging).

For live cell staining, axons elongating into the microtunnels were stained with CellTrace Calcein Red-Orange AM dye (Thermo Fisher Scientific). Briefly, 0.5 µM of the dye was diluted in neural media and added to the cultured cells for 1 h at 37 ºC. Cells were then washed twice with fresh neural media (without the dye). Confocal imaging was performed using an LSM 780 laser scanning confocal microscope (Zeiss).

2.11. Statistical analyses

Statistical analyses were performed using Prism 5 for Windows (GraphPad Software, Inc.) and SPSS Statistics 25 (IBM). Differences in fluorescein concentration were analysed with one-way analysis of variance (ANOVA) and Tukey's multiple comparison *post hoc* test. Differences in medium pH and osmolality were analysed with ANOVA for repeated measures. The effects of drugs in pharmacological tests were evaluated with the Friedman test and Wilcoxon signed-rank *post hoc* test with Bonferroni's corrections. Differences between compartments after each treatment were evaluated with the Kruskal-Wallis test. A p value < 0.05 was considered significant.

3. RESULTS AND DISCUSSION

3.1. Configurations for custom MEAs and microfluidic device

The basic concept of MEMO is that seizure-like activity of hPSC-derived neuronal networks is monitored with MEA technology in three separate but axonally connected compartments forming a functional circuitry (Fig. 1a). Contrary to other devices with three or more compartments (Dworak and Wheeler, 2009; Park, Jaewon et al., 2012; van de Wijdeven et al., 2018; Ristola et al., 2019), all three compartments in MEMO are interconnected to each other in a loop format, enabling functional circuitry formation. To our knowledge, this configuration has been reported only once earlier, albeit with microcontact printing (Dauth et al., 2017) which does not, however, allow easy targeting of pharmacological treatments to compartments.

Standard n × n electrode layouts of commercial MEAs can be integrated with simple microfluidic devices (Pan et al., 2011; Habibey et al., 2015; Hong et al., 2017), but for more complex devices such as MEMO, custom-designed MEAs (Dworak and Wheeler, 2009; Moutaux et al., 2018) are a necessity. From the MEA design and fabrication point of view, the main challenge lies in finding meaningful routes and adequate space for all electrode tracks. Thus, we found it rational to optimise the microfluidic device first for the biological research question and then design and fabricate the MEA. The median impedances of the circular (n = 504) and rectangular electrodes (n = 72) were

217 kΩ and 101 kΩ, respectively. These were in the same range with earlier in-house made as well as commercial MEAs (Ryynänen et al., 2018).

When combining microfluidic devices and MEA technologies, suboptimal attachment of MEA and PDMS surfaces can result in medium leakage or unwanted neurite growth under the PDMS (Morin et al., 2006). We have observed that the uneven surface of the MEA, caused by the track and electrode profiles, can contribute to poor MEA-PDMS attachment. Therefore, two alternative electrode layouts (electrodes measuring the neuronal activity in microtunnels located either in front or under the microtunnels) and irreversible bonding (Park, Jeong Won et al., 2006) were considered to improve the attachment. Manual alignment of the MEAs with the channel layout of the microfluidic device (Fig. 1d) was successful, though with custom MEA version 2 the microtunnel electrodes were occasionally positioned partially under, and not in front of the microtunnels as intended. As custom MEA version 1 was easier to align with the microtunnels, it was therefore chosen for further use. Altogether, all MEAs and microfluidic devices were successfully integrated with sufficient alignment and attachment, without medium leakage or unwanted neurite growth under the PDMS.

To perform pharmalogical tests, the compartments need to be fluidically well isolated (Taylor, Anne M. et al., 2005; Park, Jaewon et al., 2009). The fluidic isolation between compartments containing cells was analysed by following the diffusion of fluorescein Na salt from Compartment 1 to the adjacent compartments (Fig. 3a,b). The mean fluorescein concentrations after 1 h were 52.32 µM in Compartment 1, 0.08 µM in Compartment 2 and 0.31 µM in Compartment 3 ([$F(2, 6) = 34305$, $p < 0.0001$]; Fig. 3b). No significant diffusion was detected even in devices with no cells (Fig. S2). The results show that the compartments are fluidically well isolated and MEMO is therefore suitable for pharmacological manipulations.

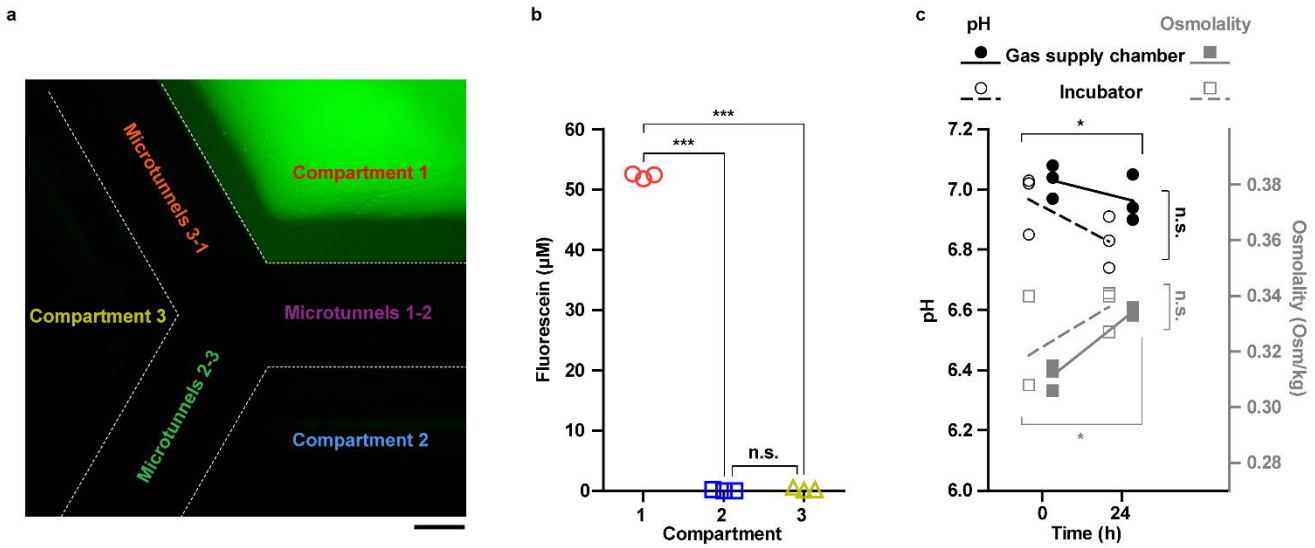

Fig. 3. | **Fluidic isolation and maintenance of medium pH and osmolality in MEMO. a,** Fluorescein Na salt (50 µM) was added to Compartment 1 and visualised under a fluorescence microscope after 1 h. The scale bar is 200 µm. **b,** Fluorescein concentration in different compartments was quantified by measuring the absorbance of the medium at 490 nm. Statistical significance was tested with one-way analysis of variance (ANOVA) and Tukey's multiple comparison *post hoc* test. *n* = 3. **c,** Medium pH and osmolality in MEMO were measured after keeping the device on a heated MEA headstage under the gas supply chamber or in an incubator in standard cell culture conditions for 24 h. Please note that the groups are horizontally shifted to differentiate them. Group means are connected by lines. *n* = 3**.** Statistical significances were tested with ANOVA for repeated measures. * $p < 0.05$; ** $0.01 > p > 0.001$; *** $p < 0.001$; n.s. = not significant.

3.2. Performance of gas supply system

MEMO includes a gas supply chamber that feeds the platform with 5 % CO_2 during prolonged MEA recordings (Fig. 1e,f) in order to maintain proper pH and osmolality (Halldorsson et al., 2015). A PDMS gasket tightens the junction between the chamber and the MEA. A sterile plastic lid (thickness 100 µm, ⌀ 24 mm) placed on the medium reservoir prevented contamination and evaporation during recordings.

To evaluate the performance of the gas supply system, we measured the pH and osmolality of the medium before and after 24 h of continuous recording on the MEA headstage (Fig. 3c; corresponding MEA data in. Fig. S3). There were no differences in medium pH [$F(1, 4) = 2.582$, $p = 0.1833$)] or osmolality [$F(1, 4) = 0.4281$, $p = 0.5486$] between the platforms used with the gas supply system and platforms kept in an incubator (Fig. 3c). There were statistically significant changes in pH [$F(1, 4) = 19.03$, $p = 0.0120$] and osmolality [$F(1, 4) = 17.04$, $p = 0.0145$] over time. Under the gas supply system, the pH decreased from 7.03 to 6.96, and the osmolality increased from 0.311 to

0.334 Osm/kg. Nevertheless, the changes were the same in the incubator, and the time × environment control type interaction was not significant to pH [$F(1, 4) = 2.396$, $p = 0.1966$] or osmolality, [$F(1, 4) = 0.3364$, $p = 0.5930$]. Thus, the gas supply system can maintain medium pH and osmolality similar to an incubator for at least 24 h.

3.3. Differentiation and maturation of neuronal cultures

Neuronal cell aggregation or detachment can be an issue in microfluidic devices during long-term culturing (Shimba et al., 2019). Here, the neuronal cultures in MEMO were considered healthy, with only minor cell aggregation at the time of pharmacological experiments on DOM 55-62. The MEMOs followed up to 98 days displayed more prominent cell aggregation, whereas cell detachment or death was not observed. The axonal growth in microtunnels was stable, and no retractions were observed. The microtunnel (Fig. 4a) and compartment regions were imaged after immunofluorescence staining. The cultures expressed both axonal (Fig. 4b,b′,d) and dendritic markers (Fig. 4c,d) in all compartments evenly. With calcein-AM staining, the axons growing through the microtunnels were easily visible (Fig. 4e). The axonal growth *via* microtunnels was further confirmed by TUBB3 and NF-H staining (Fig. 4f). The cultures contained both inhibitory and excitatory neurons (Fig. 4h). Furthermore, expression of both pre- and postsynaptic terminal markers was detected (Fig. 4i), all suggesting for mature network stage (Shi et al., 2012). Long-term neuronal cultures also contained astrocytes important for functional maturation of neuronal networks (Fig. 4g, (Paavilainen et al., 2018). The results confirmed the development of viable neuronal networks, connected circuitry and their long-term sustainability in MEMO.

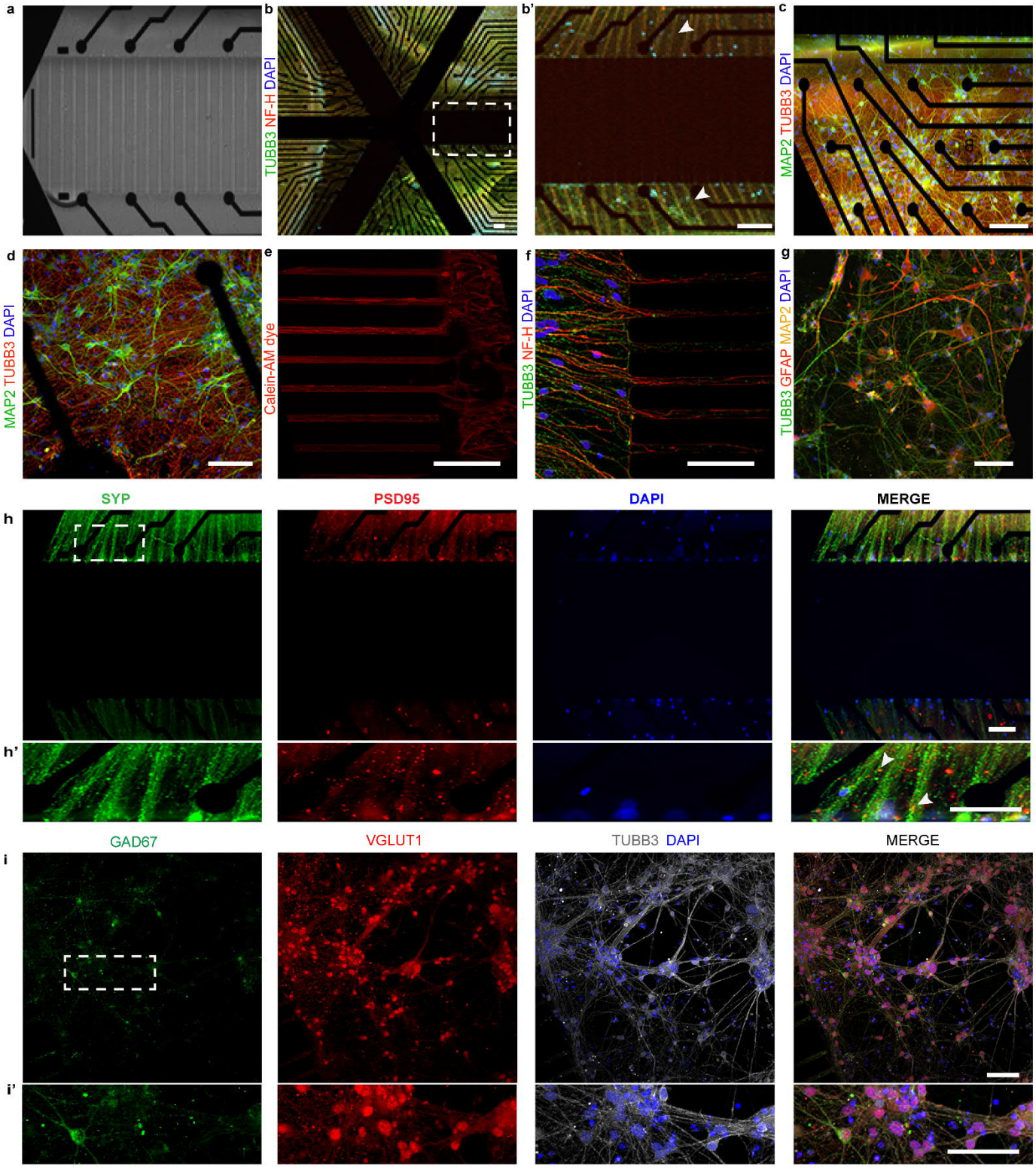

Fig. 4. | **Characterisation of neurons in MEMO. a,** Phase contrast showing the microtunnel region. **b,** (**b′** enlarged image of square area in **b**), Overview of MEMO platform showing immunofluorescent image of neurons (TUBB3 and NF-H) visible in all three cell compartments, as well as growth of axons into the microtunnels. **b′** shows axon bundles entering the microtunnels (white arrows). **c**,**d**, Immunofluorescent images of neuronal networks (MAP2 and TUBB3) present in proximity to the compartment electrodes. **e,** Axons in the microtunnels were stained with calcein dye (red, DOM49) used for labelling of live cells. **f,** TUBB3 (green) and NF-H (red) positive axons penetrate extensively through the microtunnels (DOM 15). **g,** Few GFAP-positive astrocytes (red) were observed in the neuronal culture (MAP2 and TUBB3) on DOM 62. **h,** Mature neurons expressing both pre- (SYP, green) and post- (PSD95, red) synaptic markers (DOM 62). **i,** Neurons expressed GAD67 (green, enzyme essential for GABA production), as well as VGLUT1 (red,

glutamate transporter 1), **h′** and **i′** are enlarged images of **h** and **i,** respectively. Arrows in **h′** show localisation of SYP and PSD95. DAPI nuclear stain is in blue. All scale bars are 200 µm.

3.4. Development of network activity in MEMO

The functional maturation of hPSC-derived neuronal cultures can take several weeks on MEA's (Odawara et al., 2016; Shimba et al., 2019). Thus, in this study, we monitored the electrical activity of the hPSC-derived networks with the integrated MEAs for 98 days to verify their functional development and functional circuitry formation (Fig. 5). The spontaneous activity gradually increased, and synchronous bursts spanning all three compartments were evident after DOM 49 (Fig. 5a-d). Synchronous bursts are generally considered as an indication of functional maturity (Odawara et al., 2016; Shimba et al., 2019) and connectivity (Kamioka et al., 1996) in MEA recordings. Here, we concentrate on the data combined from all compartment electrodes in each MEMO. The median number of active electrodes reached 44/72 (61 %) by the time the synchronous bursts were evident on DOM 49 and was at its highest, 64/72 (83 %), on DOM 84 (Fig. 5g). The mean firing rate in active electrodes was 3.3 Hz on DOM 49 and reached a maximum of 7.8 Hz, on DOM 70 (Fig. 5h). Additionally, the compartment-specific results are shown in Fig. 5g-n. Overall, the development of these basic functional parameters shows that MEMO supports development and long-term maintenance of neuronal function.

The spike train tiling coefficient (STTC) is a measure of network synchronisation that calculates the proportion of spikes detected by an electrode that happen near-simultaneously with spikes of a another electrode, and performs the calculation for all electrode pairs in a given network (Cutts and Eglen, 2014; Gelfman et al., 2018). The STTC value between all compartment electrodes remained at 0 up to DOM 31 but rose to 0.16 at the advent of synchronous bursts on DOM 49 and reached 0.54 by DOM 98 (Fig. 5i). The increase in STTC confirms that synchronous network activity develops between the three compartments in MEMO. Functional connections of rodent neurons in a similar configuration have been established earlier (Dauth et al., 2017), but synchronous activity between three physically separated networks on MEA has not been shown earlier, especially with human networks. The synchronous bursts and the increase in quantified synchrony show that MEMO

represents an ensemble of interconnected networks, similar to the human brain with seizure manifestation (Centeno and Carmichael, 2014; Englot et al., 2015; Fisher et al., 2017)

The number of burst-detecting electrodes slowly rose to 5/72 (7 %) by DOM 38 but increased to 21/72 (29 %) on DOM 49 when the synchronous bursts appeared and reached as high as 51/72 (71 %) on DOM 77 (Fig. 5j). Before the emergence of synchronous bursts, the number of bursts in burst-detecting electrodes was variable and high, reaching 14.3 bursts per min on DOM 38 (Fig. 5k). When bursts synchronised on DOM 49, the number of bursts stabilised to 6.2 per min, and steadily decreased to 2.1 per min by DOM 98. Burst duration increased over time from 0.4 s on DOM 38 to 2.6 s on DOM 98 (Fig. 5l). The number of spikes per burst followed the same trend, increasing from 11 on DOM 38 to 118 on DOM 98 (Fig. 5m). The spike frequency in bursts also increased from 19 Hz on DOM 3 up to 46 Hz on DOM 70 (Fig. 5n). The stabilisation of burst counts and the increase in burst size show that MEMO supports the development of burst activity in hPSC-derived networks. In contrast to previous work with rodent cortical neurons in a 3-nodal microfluidic chip (van de Wijdeven et al., 2019), the spike frequencies and burst counts here were substantially higher. Most likely this reflects the biological differentiation and maturation of used cell types (Hyvarinen et al., 2019), but one can also speculate that the current 3-compartment loop structure better mimics natural circuitry formation.

As shown previously (Dworak and Wheeler, 2009; Pan et al., 2014; Habibey et al., 2015), the microtunnels increase the signal amplitude in the electrodes underneath (Fig. 5e; Fig. S4). The strong signal amplification caused aberrant and highly different results between the microtunnel electrodes of the two custom MEA versions (. Fig. S5 and S6). Thus, analyses are concentrated on the compartment electrodes. Nevertheless, the network activity development was also observed with the microtunnel electrodes (Fig. 5a-d), verifying that the synchronous activity between compartments is mediated by the axons in microtunnels. Taken together, the results show that synchronous network activity between the compartments develops over time and that MEMO maintains functional neuronal networks for at least 98 days.

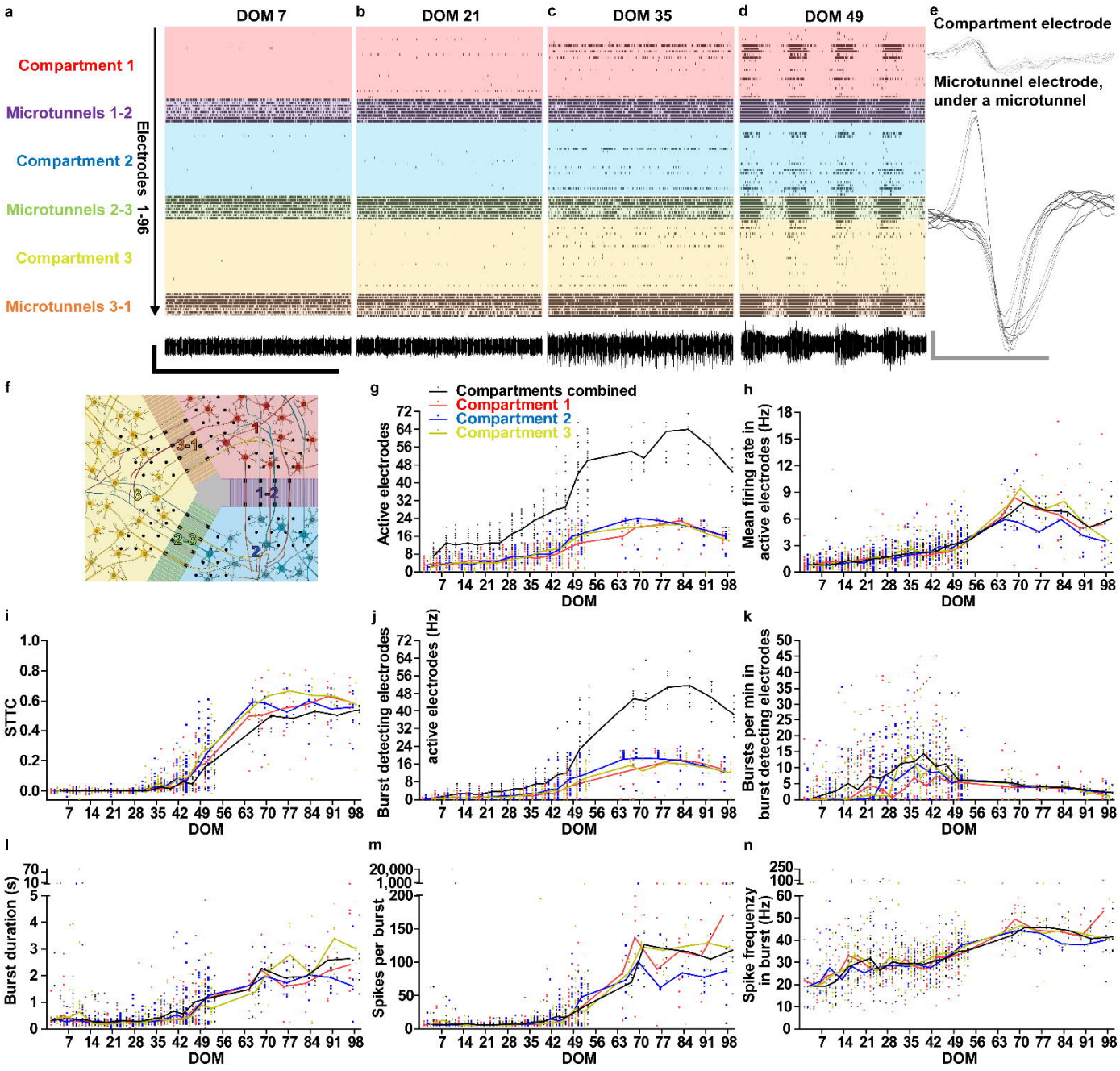

Fig. 5.| **Development of network activity in MEMO**. **a**,**b**,**c**,**d** Representative 30 s raster plots showing the development of network activity from DOM 7 to DOM 49 (the example recorded with custom MEA version 1). The corresponding signal from an individual compartment electrode is shown underneath each raster plot. The scale bars correspond to 50 µV (vertical) and 30 s (horizontal). **e**, Overlays of 10 consecutive spikes (DOM 49) from individual compartment and microtunnel electrodes. The scale bars correspond to 50 µV (vertical) and 1 ms (horizontal). **f**, A concept image of the compartments and microtunnels along with a colour code for **a-d**. **g**, Number of active electrodes, i.e., electrodes detecting spikes. **h**, Mean firing rate in active electrodes describes the overall spiking activity of the networks. **i**, Spike train tiling coefficient (STTC) describes synchrony of the network activity. **j**, Number of electrodes that detect bursts. **k**, Number of bursts per minute in burst-detecting electrodes. **l**, Burst duration. **m**, Number of spikes per burst. **n**, Spike frequency in burst. The quantified results in **g-m** are presented for each compartment separately and for all compartment electrodes combined. Please note that the groups are horizontally shifted to differentiate them and that the upper part of the split y-axis in **l-n** have different scaling. Lines connect the group medians. Data from the two custom MEA versions are pooled. DOM 3-52: $n_{\text{Custom MEA version 1}} = 11$, $n_{\text{Custom MEA version 2}} = 10$, $n_{\text{total}} = 21$. DOM 66-98: $n_{\text{Custom MEA version 1}} = 2$, $n_{\text{Custom MEA version 2}} = 5$, $n_{\text{total}} = 7$.

3.5. Induction of seizure-like events in MEMO

The convulsant, KA, and anticonvulsant, PHT, were tested in MEMO on DOM 55-62 (Fig. 6) to see their effect on spontaneous network activity. While the bursts mark the development of network functionality (Wagenaar et al., 2006; Odawara et al., 2016), they are also considered as seizure-like events in MEA recordings (Odawara et al., 2016; Chong et al., 2018; Liu et al., 2019). KA was added to Compartment 1 (Fig. 6a,b,d,e) in which the number of bursts per minute in burst-detecting electrodes increased to 214 % from baseline (Fig. 6g) as also shown earlier (Odawara et al., 2016). Although some changes in burst counts of individual electrodes could be observed in the neighbouring compartments (Fig. 6d vs. e), the increase in the average number of bursts per compartment occurred only in Compartment 1 ($p = 0.020$; Fig. 5g). KA also reduced the number of burst-detecting electrodes to 50 % from baseline ($p = 0.014$) locally in Compartment 1 ($p = 0.020$; Fig. 6h). KA had no effect on the mean firing rate in active electrodes (Fig. 6i) but it did reduce the number of active electrodes to 73 % from baseline, although the effect was not statistically significant (Fig. 6j). Taken together, KA increased burst activity in targeted areas of a network while silencing others (Fig. 6d vs. e), and the effects remained focal in the compartment that was treated.

Next, PHT was added to Compartment 2. PHT had no clear effects on the number of bursts per minute in burst-detecting electrodes (Fig. 6g) or on the number of burst-detecting electrodes (Fig. 6h, Fig. 6e vs. f). Instead, PHT reduced the mean firing rate in active electrodes to 57 % from baseline, and the effect was localised to the treated compartment ($p = 0.023$; Fig. 6i). PHT also reduced the number of active electrodes in Compartment 2 to 82 % of baseline ($p = 0.040$; Fig. 6j). Taken together, PHT reduced the overall spike activity of the network, but contrary to earlier MEA data from hPSC dericed networks (Odawara et al., 2016) and rat organotypic cultures (Chong et al., 2018; Liu et al., 2019), it had little effect on the occurrence of bursts. This suggests that the burst activity in the PHT-treated compartment was maintained by the functional connections from the other compartments.

We also performed another set of experiments where, following KA treatment in Compartment 1, PHT was added to Compartments 2 and 3 (Fig. S7). The experiment reproduced the trends in Fig. 6, but in one of the repeats bursting throughout all three compartments became more synchronous after adding KA to Compartment 1 (Fig. S7a-c). Overall, the synchronous bursts spanning all three compartments were present even during treatments (Fig. 6a-c,. Fig. S7a-c), indicating persistent functional inter-compartment connectivity. The convulsant and anticonvulsant effects in MEMO were easy to detect and the seizure-like events remained primarily localised to the treated compartment. This is similar to focal epilepsy, where seizures localise to specific networks (Du and Parent, 2015; Englot et al., 2015; Fisher et al., 2017). To our knowledge, MEMO is the first platform where seizure-like events localise to a predefined subset of functionally connected human neuronal networks, thus mimicking focal epilepsy.

Even though the seizure-like events were focal, there were also indications in individual electrodes and in one individual MEMO that convulsant-induced changes in seizure type burst patterns can spread between compartments. This leads us to hypothesise that if the baseline excitability of the networks is increased with an epilepsy mutation (McSweeney et al., 2016) or Mg^{2+} depletion (Grainger et al., 2018), the seizure-like events would spread frequently between compartments. However, extensive work will be needed to verify this hypothesis.

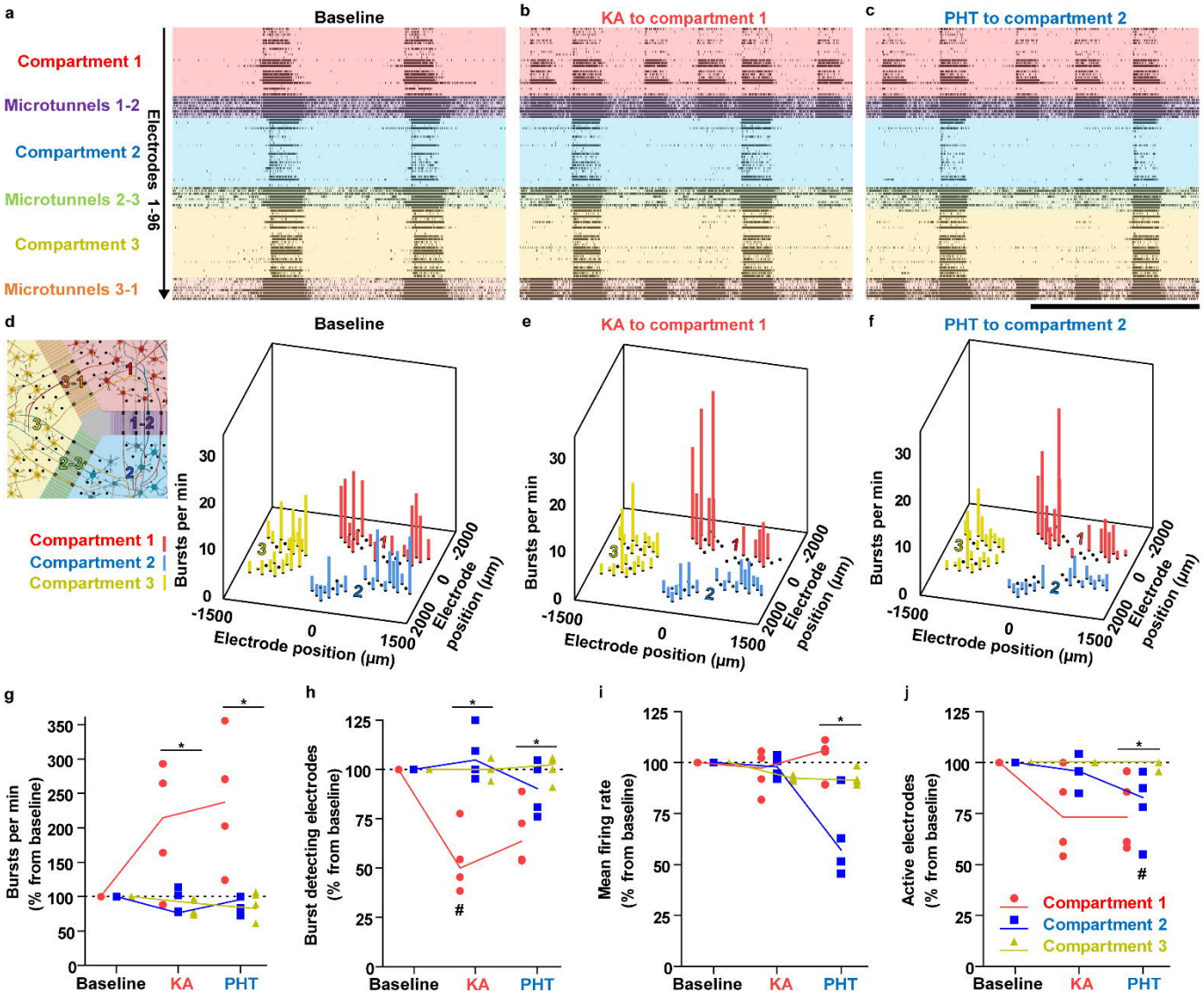

Fig. 6. | Effects of kainic acid and phenytoin in MEMO. a,**b**,**c** Representative raster plots from a baseline recording (**a**), after adding 5 µM kainic acid (KA) to Compartment 1 (**b**) and after adding 50 µM phenytoin (PHT) to Compartment 2 (**c**). The representative set was recorded on DOM 58. The scale bar in **c** (applying to **a-c**) is 30 s. **d**, On the left, a concept image of the compartment layout. On the right, quantification of bursts per min in each compartment electrode during a baseline recording (shown in **a**). **e**, Number of bursts per min in each compartment electrode after the addition of KA to Compartment 1 (shown in **b**). **f**, Number of bursts per min in each compartment electrode after the addition of PHT to Compartment 2 (shown in **c**). **g**, Effects of the treatments on the number of bursts per minute in burst-detecting electrodes. **h**, Effects of the treatments on the number of burst-detecting electrodes. **i**, Effects of the treatments on the mean firing rate in active electrodes. **j**, Effects of the treatments on the number of active electrodes. The results in **g-j** are calculated as percent from baseline, and the solid lines connect compartment medians. # $p < 0.05$ (Wilcoxon signed-rank *post hoc* test with Bonferroni's corrections against baseline after the Friedman test). * $p < 0.05$ (Kruskal-Wallis test). $n = 4$.

4. CONCLUSIONS

We conclude that MEMO supports the structural and functional development of human neuronal networks and enables culture periods of more than three months. In terms of applicability, MEA-PDMS attachment in MEMO is perfected, pharmacological manipulations are easy to perform and continuous MEA recordings of several hours can be performed at the bench. The networks can be monitored with a microscope as well as fixed and stained. Data from the integrated custom MEA show that the three separated networks form functional axonal connections through the microtunnels, which enables synchronous electrical activity between the networks connected in closed chain configuration mimicking functional circuitry. Seizure-like events can be induced and targeted to specific networks, and MEMO can therefore model focal seizures in human neuronal networks.

CONFLICT OF INTERESTS

SN and LS are co-inventors in a patent application relating to work in this manuscript. The remaining authors declare no competing interests.

AUTHOR CONTRIBUTIONS

AP and RM performed the experiments; LS designed and produced the microfluidic device; TR designed and fabricated the custom MEAs; JK designed and produced the gas supply system; TH designed the cell differentiation; AV and LA developed the MEA data analysis; JL, PK and SN supervised the work; AP drafted the manuscript which all authors supplemented.

ACKNOWLEDGEMENTS

This research was funded by Business Finland, Academy of Finland (decision No. 311017, 311021 and 311022), Juliana von Wendt fund (AP) and Finnish Epilepsy Research Foundation (RM). The work was supported by the Imaging Facility, Facility of Electrophysiological Measurements and iPS Cells Facility (Faculty of Medicine and Health Technology, Tampere University), as well as Fablab Tampere (Tampere University). The authors also thank Biocenter Finland for the support of Imaging and iPS cells facilities. Thanks to Dr Sanna Hagman, Juha Heikkilä, Eija Hannuksela and Hanna Mäkelä for technical assistance, Outi Paloheimo for artwork, Dr Teemu Ihalainen for advice on

fluorescein analysis, Dr Stephen Eglen for advice with meaRtools and Dr Mervi Ristola for advice on microfluidic devices.

References

Brighi, F. Cordella, L. Chiriatti, A. Soloperto, S. Di Angelantonio, 2020. Retinal and Brain Organoids: Bridging the Gap Between in vivo Physiology and in vitro Micro-Physiology for the Study of Alzheimer's Diseases, Frontiers in neuroscience. 14 655.

Centeno, D.W. Carmichael, 2014. Network Connectivity in Epilepsy: Resting State fMRI and EEG-fMRI Contributions, Front. Neurol. 5 93.

Chong, S. Balosso, C. Vandenplas, G. Szczesny, E. Hanon, K. Claes, et al., 2018. Intrinsic Inflammation Is a Potential Anti-Epileptogenic Target in the Organotypic Hippocampal Slice Model, Neurotherapeutics. 15 (2), 470-488.

Comina, A. Suska, D. Filippini, 2014. PDMS lab-on-a-chip fabrication using 3D printed templates, Lab Chip. 14 (2), 424-430.

Cutts, S.J. Eglen, 2014. Detecting Pairwise Correlations in Spike Trains: An Objective Comparison of Methods and Application to the Study of Retinal Waves, J. Neurosci. 34 (43), 14288-14303.

Dauth, B.M. Maoz, S.P. Sheehy, M.A. Hemphill, T. Murty, M.K. Macedonia, et al., 2017. Neural Circuits Neurons derived from different brain regions are inherently different in vitro: a novel multiregional brain-on-a-chip, J.Neurophysiol. 117 (3), 1320-1341.

Du, J.M. Parent, 2015. Using Patient-Derived Induced Pluripotent Stem Cells to Model and Treat Epilepsies, Curr. Neurol. Neurosci. Rep. 15 (10), 71.

Dworak, B.C. Wheeler, 2009. Novel MEA platform with PDMS microtunnels enables the detection of action potential propagation from isolated axons in culture, Lab Chip. 9 (3), 404-410.

Englot, L.B. Hinkley, N.S. Kort, B.S. Imber, D. Mizuiri, S.M. Honma, et al., 2015. Global and regional functional connectivity maps of neural oscillations in focal epilepsy, Brain. 138 2249-2262.

Fiest, K.M. Sauro, S. Wiebe, S.B. Patten, C. Kwon, J. Dykeman, et al., 2017. Prevalence and incidence of epilepsy: A systematic review and meta-analysis of international studies, Neurology. 88 (3), 296-303.

Fisher, J.H. Cross, J.A. French, N. Higurashi, E. Hirsch, F.E. Jansen, et al., 2017. Operational classification of seizure types by the International League Against Epilepsy: Position Paper of the ILAE Commission for Classification and Terminology, Epilepsia. 58 (4), 522-530.

Gelfman, Q. Wang, Y. Lu, D. Hall, C.D. Bostick, R. Dhindsa, et al., 2018. meaRtools: An R package for the analysis of neuronal networks recorded on microelectrode arrays, Plos Comput. Biol. 14 (10), e1006506.

Golyala, P. Kwan, 2017. Drug development for refractory epilepsy: The past 25 years and beyond, Seizure. 44 147-156.

Grainger, M.C. King, D.A. Nagel, H.R. Parri, M.D. Coleman, E.J. Hill, 2018. In vitro Models for Seizure-Liability Testing Using Induced Pluripotent Stem Cells, Front. Neurosci. 12 590.

Habibey, A. Golabchi, S. Latifi, F. Difato, A. Blau, 2015. A microchannel device tailored to laser axotomy and long-term microelectrode array electrophysiology of functional regeneration, Lab Chip. 15 (24), 4578-4590.

Halldorsson, E. Lucumi, R. Gómez-Sjöberg, R.M.T. Fleming, 2015. Advantages and challenges of microfluidic cell culture in polydimethylsiloxane devices, Biosens. Bioelectron. 63 218-231.

Hong, S. Joo, Y. Nam, 2017. Characterization of Axonal Spikes in Cultured Neuronal Networks Using Microelectrode Arrays and Microchannel Devices, IEEE T. Bio-med. Eng. 64 (2), 492-498.

Hongisto, T. Ilmarinen, M. Vattulainen, A. Mikhailova, H. Skottman, 2017. Xeno- and feeder-free differentiation of human pluripotent stem cells to two distinct ocular epithelial cell types using simple modifications of one method, Stem Cell Res. Ther. 8 291.

Hyvarinen, A. Hyysalo, F.E. Kapucu, L. Aarnos, A. Vinogradov, S.J. Eglen, et al., 2019. Functional characterization of human pluripotent stem cell-derived cortical networks differentiated on laminin-521 substrate: comparison to rat cortical cultures, Sci.Rep. 9 (1), 17125-8.

Johnstone, G.W. Gross, D.G. Weiss, O.H.-. Schroeder, A. Gramowski, T.J. Shafer, 2010. Microelectrode arrays: A physiologically based neurotoxicity testing platform for the 21st century, Neurotoxicology. 31 (4), 331-350.

Kamioka, E. Maeda, Y. Jimbo, H.P.C. Robinson, A. Kawana, 1996. Spontaneous periodic synchronized bursting during formation of mature patterns of connections in cortical cultures, Neurosci. Lett. 206, 2 109-112.

Kreutzer, L. Yla-Outinen, P. Karna, T. Kaarela, J. Mikkonen, H. Skottman, et al., 2012. Structured PDMS Chambers for Enhanced Human Neuronal Cell Activity on MEA Platforms, J. Bionic Eng. 9 (1), 1-10.

Lancaster, N.S. Corsini, S. Wolfinger, E.H. Gustafson, A.W. Phillips, T.R. Burkard, et al., 2017. Guided self-organization and cortical plate formation in human brain organoids, Nat. Biotechnol. 35 (7), 659-666.

Lappalainen, M. Salomaki, L. Yla-Outinen, T.J. Heikkila, J.A.K. Hyttinen, H. Pihlajamaki, et al., 2010. Similarly derived and cultured hESC lines show variation in their developmental potential towards neuronal cells in long-term culture, Regen. Med. 5 (5), 749-762.

Lieb, H. Stark, C. Thielemann, 2017. A stationary wavelet transform and a time-frequency based spike detection algorithm for extracellular recorded data, J. Neural Eng. 14 (3), 036013.

Liu, A.R. Sternberg, S. Ghiasvand, Y. Berdichevsky, 2019. Epilepsy-on-a-Chip System for Antiepileptic Drug Discovery, IEEE T. Bio-med. Eng. 66 (5), 1231-1241.

Mayer, O. Arrizabalaga, F. Lieb, M. Ciba, S. Ritter, C. Thielemann, 2018. Electrophysiological investigation of human embryonic stem cell derived neurospheres using a novel spike detection algorithm, Biosens.Bioelectron. 100 462-468.

McSweeney, A.B. Gussow, S.S. Bradrick, S.A. Dugger, S. Gelfman, Q. Wang, et al., 2016. Inhibition of microRNA 128 promotes excitability of cultured cortical neuronal networks, Genome Res. 26 (10), 1411-1416.

Metsälä, J. Kreutzer, H. Hogel, P. Miikkulainen, P. Kallio, P.M. Jaakkola, 2018. Transportable system enabling multiple irradiation studies under simultaneous hypoxia in vitro, Radiat. Oncol. 13 220.

Morin, N. Nishimura, L. Griscom, B. LePioufle, H. Fujita, Y. Takamura, et al., 2006. Constraining the connectivity of neuronal networks cultured on microelectrode arrays with microfluidic techniques: A step towards neuron-based functional chips, Biosens. Bioelectron. 21 (7), 1093-1100.

Moutaux, B. Charlot, A. Genoux, F. Saudou, M. Cazorla, 2018. An integrated microfluidic/microelectrode array for the study of activity-dependent intracellular dynamics in neuronal networks, Lab Chip. 18 (22), 3425-3435.

Odawara, H. Katoh, N. Matsuda, I. Suzuki, 2016. Physiological maturation and drug responses of human induced pluripotent stem cell-derived cortical neuronal networks in long-term culture, Sci. Rep. 6 26181.

Paavilainen, A. Pelkonen, M.E.-. Mäkinen, M. Peltola, H. Huhtala, D. Fayuk, et al., 2018. Effect of prolonged differentiation on functional maturation of human pluripotent stem cell-derived neuronal cultures, Stem Cell Research. 27 151-161.

Pan, S. Alagapan, E. Franca, G.J. Brewer, B.C. Wheeler, 2011. Propagation of action potential activity in a predefined microtunnel neural network, J. Neural Eng. 8 (4), 046031.

Pan, S. Alagapan, E. Franca, T. DeMarse, G.J. Brewer, B.C. Wheeler, 2014. Large Extracellular Spikes Recordable From Axons in Microtunnels, IEEE T. Neur. Sys. Reh. 22 (3), 453-459.

Park, H. Koito, J. Li, A. Han, 2012. Multi-compartment neuron-glia co-culture platform for localized CNS axon-glia interaction study, Lab Chip. 12 (18), 3296-3304.

Park, H. Koito, J. Li, A. Han, 2009. Microfluidic compartmentalized co-culture platform for CNS axon myelination research, Biomed.Microdevices. 11 (6), 1145-1153.

Park, B. Vahidi, A.M. Taylor, S.W. Rhee, N.L. Jeon, 2006. Microfluidic culture platform for neuroscience research, Nat. Protoc. 1 (4), 2128-2136.

Pasquale, S. Martinoia, M. Chiappalone, 2010. A self-adapting approach for the detection of bursts and network bursts in neuronal cultures, J.Comput.Neurosci. 29 (1-2), 213-229.

Ristola, L. Sukki, M.M. Azevedo, A.I. Seixas, J.B. Relvas, S. Narkilahti, et al., 2019. A compartmentalized neuron-oligodendrocyte co-culture device for myelin research: design, fabrication and functionality testing, J. Micromech. Microengineering. 29 (6), 065009.

Ryynänen, M. Toivanen, T. Salminen, L. Ylä-Outinen, S. Narkilahti, J. Lekkala, 2018. Ion Beam Assisted E-Beam Deposited TiN Microelectrodes-Applied to Neuronal Cell Culture Medium Evaluation, Front. Neurosci. 12 882.

Shi, P. Kirwan, J. Smith, H.P.C. Robinson, F.J. Livesey, 2012. Human cerebral cortex development from pluripotent stem cells to functional excitatory synapses, Nat.Neurosci. 15 (3), 477-U180.

Shimba, K. Sakai, S. Iida, K. Kotani, Y. Jimbo, 2019. Long-term developmental process of the human cortex revealed in vitro by axon-targeted recording using a microtunnel-augmented microelectrode array, IEEE Trans.Biomed.Eng.

Skottman, 2010. Derivation and characterization of three new human embryonic stem cell lines in Finland, In Vitro Cell. Dev.-An. 46 (3-4), 206-209.

Taylor, M. Blurton-Jones, S.W. Rhee, D.H. Cribbs, C.W. Cotman, N.L. Jeon, 2005. A microfluidic culture platform for CNS axonal injury, regeneration and transport, Nat. Methods. 2 (8), 599-605.

Taylor, S.W. Rhee, C.H. Tu, D.H. Cribbs, C.W. Cotman, N.L. Jeon, 2003. Microfluidic multicompartment device for neuroscience research, Langmuir. 19 (5), 1551-1556.

Taylor, M. Blurton-Jones, S.W. Rhee, D.H. Cribbs, C.W. Cotman, N.L. Jeon, 2005. A microfluidic culture platform for CNS axonal injury, regeneration and transport, Nat. Methods. 2 (8), 599-605.

Trujillo, R. Gao, P.D. Negraes, J. Gu, J. Buchanan, S. Preissl, et al., 2019. Complex Oscillatory Waves Emerging from Cortical Organoids Model Early Human Brain Network Development, Cell stem cell. 25 (4), 558-569.e7.

van de Wijdeven, O.H. Ramstad, U.S. Bauer, O. Halaas, A. Sandvig, I. Sandvig, 2018. Structuring a multi-nodal neural network in vitro within a novel design microfluidic chip, Biomed.Microdevices. 20 (1), 9.

van de Wijdeven, O.H. Ramstad, V.D. Valderhaug, P. Köllensperger, A. Sandvig, I. Sandvig, et al., 2019. A novel lab-on-chip platform enabling axotomy and neuromodulation in a multi-nodal network, Biosensors and Bioelectronics. 140 111329.

Wagenaar, J. Pine, S.M. Potter, 2006. An extremely rich repertoire of bursting patterns during the development of cortical cultures, Bmc Neurosci. 7 11.

SUPPLEMENTARY MATERIAL

Pharmacological experiments

Kainic acid (KA) stock was diluted in H_2O and phenytoin (PHT) in dimethyl sulfoxide. Portion of the stock diluent in the final cell culture medium never exceeded 0.083 %. The compartments treated with drugs had empty medium reservoirs, i.e., their medium volume was maintained at 60 µl. The drugs were added by replacing 1.5 µl (i.e., 2.5 %) of the medium volume with drug-containing medium. In non-treated compartments, the medium reservoir was kept half-full (total medium volume 160 µl) to prevent diffusion of drugs to the compartment (Taylor et al., 2005a). The microelectrode array (MEA) recording was paused when adding the drugs to avoid artefacts resulting from pipetting and handling of the gas supply chamber and continued immediately after placing the gas supply chamber back on. The baseline recording was followed by the addition of KA to Compartment 1. PHT was then added either to Compartment 2 alone or to Compartments 2 and 3. All recordings were 30 min in duration. After washout with fresh medium, the modular platform for epilepsy modeling in vitro (MEMO) chips were kept for further monitoring until DOM 98, apart for one which was fixed and stained after the pharmacological experiment.

MEA data analysis

The minimum number of spikes per burst was set to five, and the cutoff for inter-spike interval (ISI) and the default maximum ISI (maxISI) were set to 100 ms. A single modification was introduced to the algorithm: when the computed ISI threshold was smaller than the default maxISI, the bursts with an inter-burst interval smaller than 100 ms were merged. Spike and burst features as well as other MEA parameters such as the number of active electrodes (electrodes with > 10 spikes/min) and spike train tiling co-efficient (STTC) were computed with meaRtools (Gelfman et al., 2018). Burst features were presented only for burst detecting electrodes.

The compartment electrode data of the two custom MEA versions were pooled for quantitative analysis, as there were no differences in the signal detection properties of the compartment electrodes.

Immunocytochemistry and imaging

Immunocytochemical staining was performed with the method described earlier (Lappalainen et al., 2010), with the exceptions that in three washes after the secondary antibody treatment, 4′,6-diamidino-2-phenylindole ([DAPI] 1:5000, D9542-10MG, Sigma-Aldrich) was added to the phosphate buffered saline (PBS), and the two following washes were performed with PBS instead of phosphate buffer. Cells were then incubated with primary antibodies overnight. Thereafter, cells were washed three times for 10 min with PBS and then incubated for an hour with the following Alexa Fluor-labelled secondary antibodies (all diluted 1:200, all from Thermo Fisher Scientific): donkey anti-rabbit 488 (A21206), goat anti-chicken 488 (A11039), donkey anti-mouse 568 (A10037), goat anti-chicken 568 (A11041), donkey anti-mouse 647 (A31571) and goat anti-chicken 647 (A21449). Fluorescence imaging was performed directly after the staining, with PBS covering the stained cells, using an IX51 microscope equipped with a DP30BW camera (both from Olympus Corporation). After this, the cells were prepared for long-term storage and confocal microscopy by replacing the PBS with Vectashield (with DAPI, H-1200, Vector Laboratories, Inc.) and covering the microfluidic device with a 170 µm thick glass coverslip. Confocal imaging was performed using an LSM 780 laser scanning confocal microscope (Zeiss).

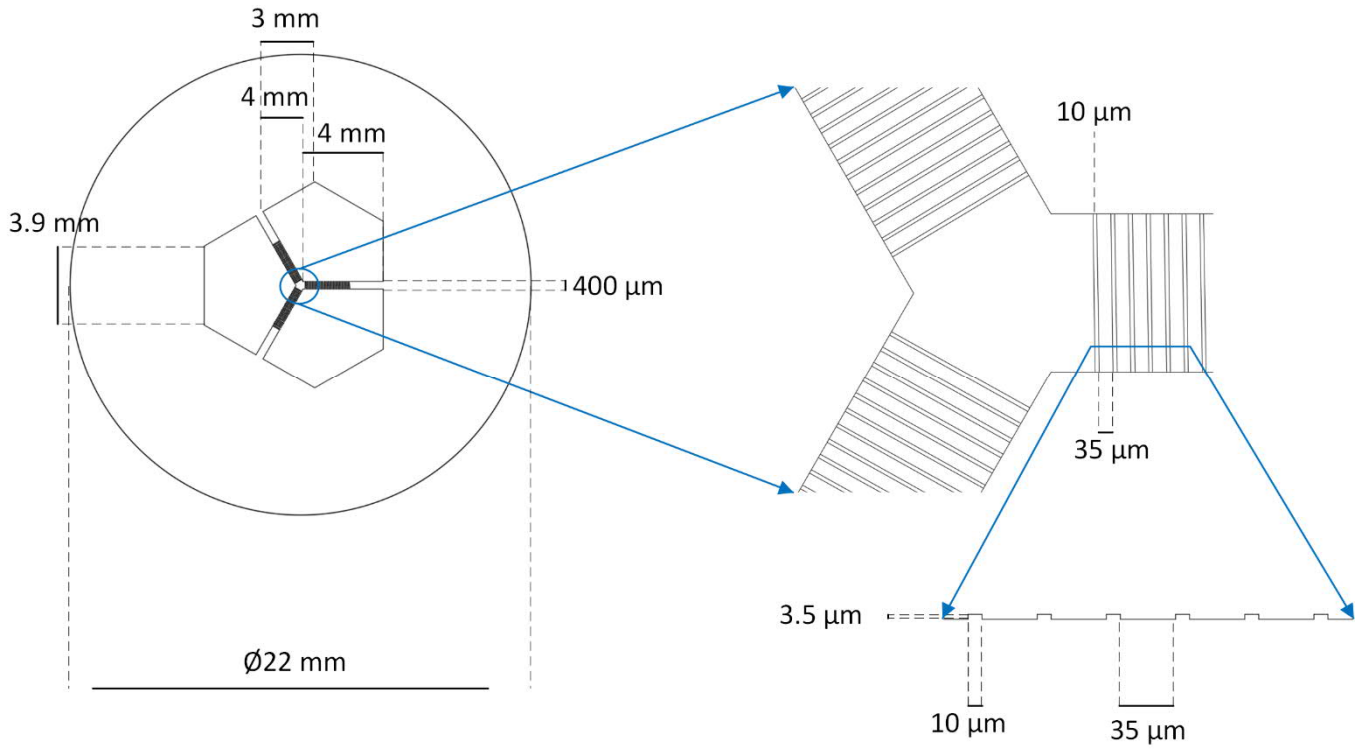

Supplementary figure 1 | Detailed dimensions of the microfluidic device. On the left the dimensions of the compartments. Height of the compartments is 3 mm. On the right the dimensions of the microtunnels as seen from above (on the top) and from the side (below).

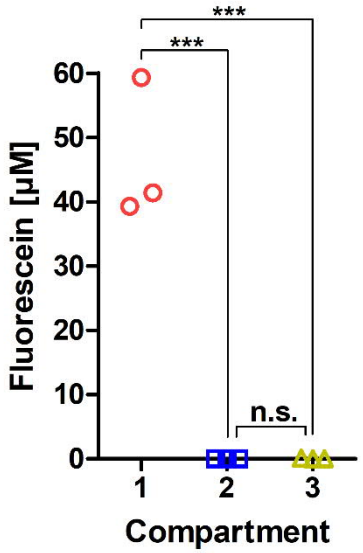

Supplementary figure 2 | Fluidic isolation in MEMO without cells. Fluorescein concentration in the three empty compartments was quantified by measuring the absorbance of the medium at 490 nm 1 h later. Statistical significance was tested with one-way analysis of variance (ANOVA) and Tukey's multiple comparison *post hoc* test. $n = 3$.

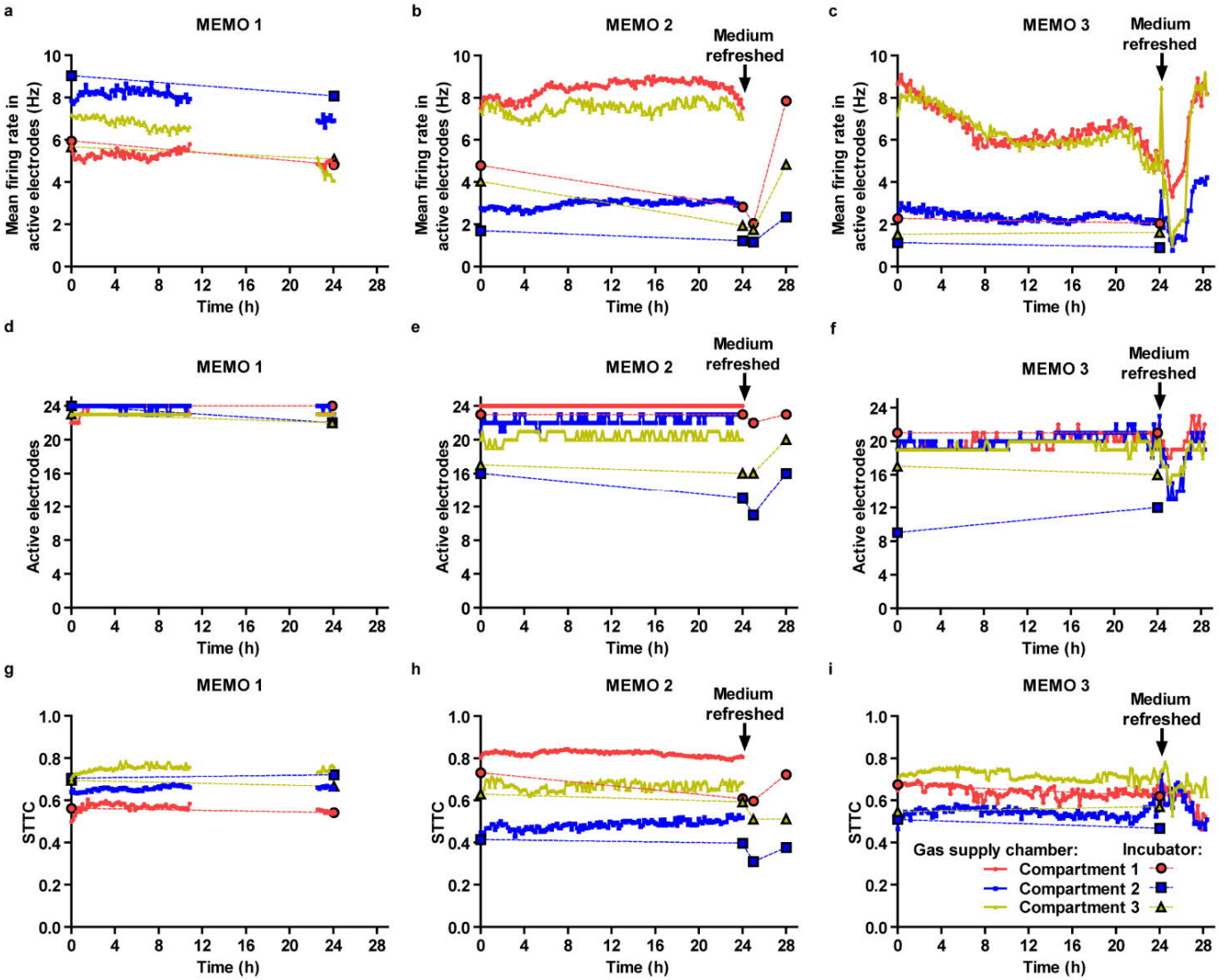

Supplementary figure 3 | Mean firing rate, active electrodes and synchrony during long-term continuous measurements with MEMO. Continuous MEA measurements were performed while testing the ability of MEMO's gas supply chamber to maintain medium pH and osmolality. Plotted here are mean firing rates in active electrodes (a,b,c), number of active electrodes (d,e,f) and spike train tiling coefficient (STTC; g,h,i) in three MEMOs (all with custom MEA version 2). The data is plotted in 10 min bins, and the controls (with the MEMOs kept in incubator between measurements) also represent 10 min recordings. With MEMO 1 (a,d,g) the recording software was crashed between 10.4 and 22.6 h due to too many windows being open simultaneously in the recording software. The problem was identified and fixed for MEMOs 2 and 3. With MEMO 2 (b,e,h), the control recordings were performed also at 25 and 28 h, i.e. 1 and 4 h after refreshing mediums, which showed that changing the medium can cause an initial depression of firing rate, followed by an increase of activity later. With MEMO 3 (c,f,i), the continuous measurement was continued until 28 h, with the medium refreshed after 24 h. The depression and increase of firing rate after refreshing medium was seen also in the continuous measurement with MEMO 3.

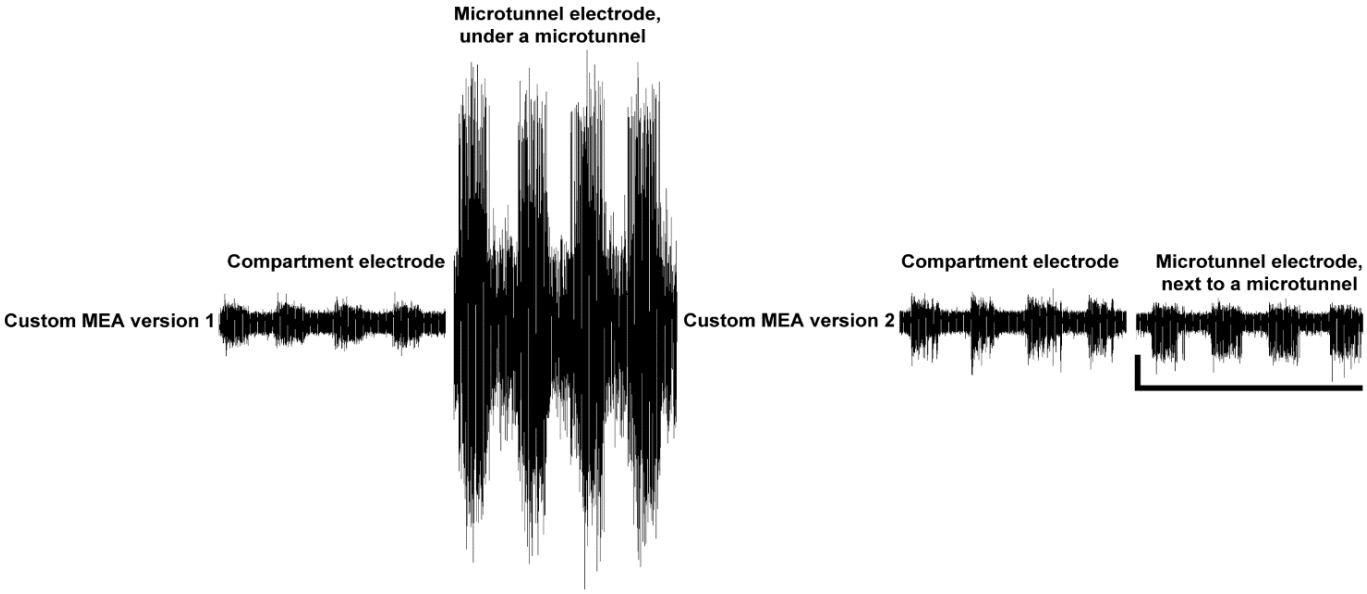

Supplementary figure 4 | Representative traces of filtered MEA signal from both custom MEA versions. The representative 30 s traces of band-pass (> 200 Hz) filtered MEA signals were recorded on DOM 49, measured with custom MEA versions 1 (left) and 2 (right). The vertical scale bar is 50 µV and the horizontal 30 s.

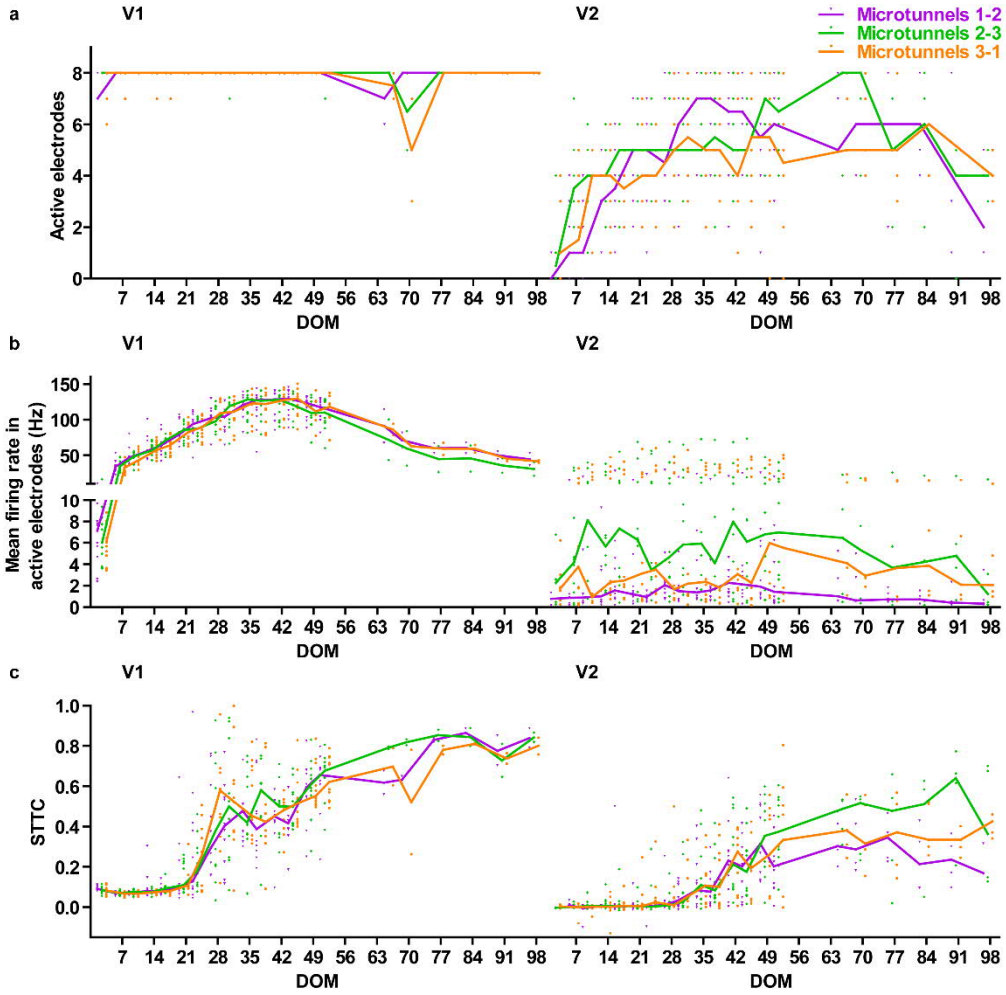

Supplementary figure 5 | Spike activity and synchrony in microtunnel electrodes. The timeline for custom MEA version 1 (V1) is on the left and the timeline for custom MEA version 2 (V2) on the right in each subfigure. **a**, Number of active electrodes. **b**, Mean firing rate in active electrodes. **c**, Spike train tiling co-efficient (STTC). Lines connect the group medians. DOM 3-52: $n_{V1} = 11$, $n_{V2} = 10$. DOM 66-98: $n_{V1} = 2$, $n_{V2} = 5$.

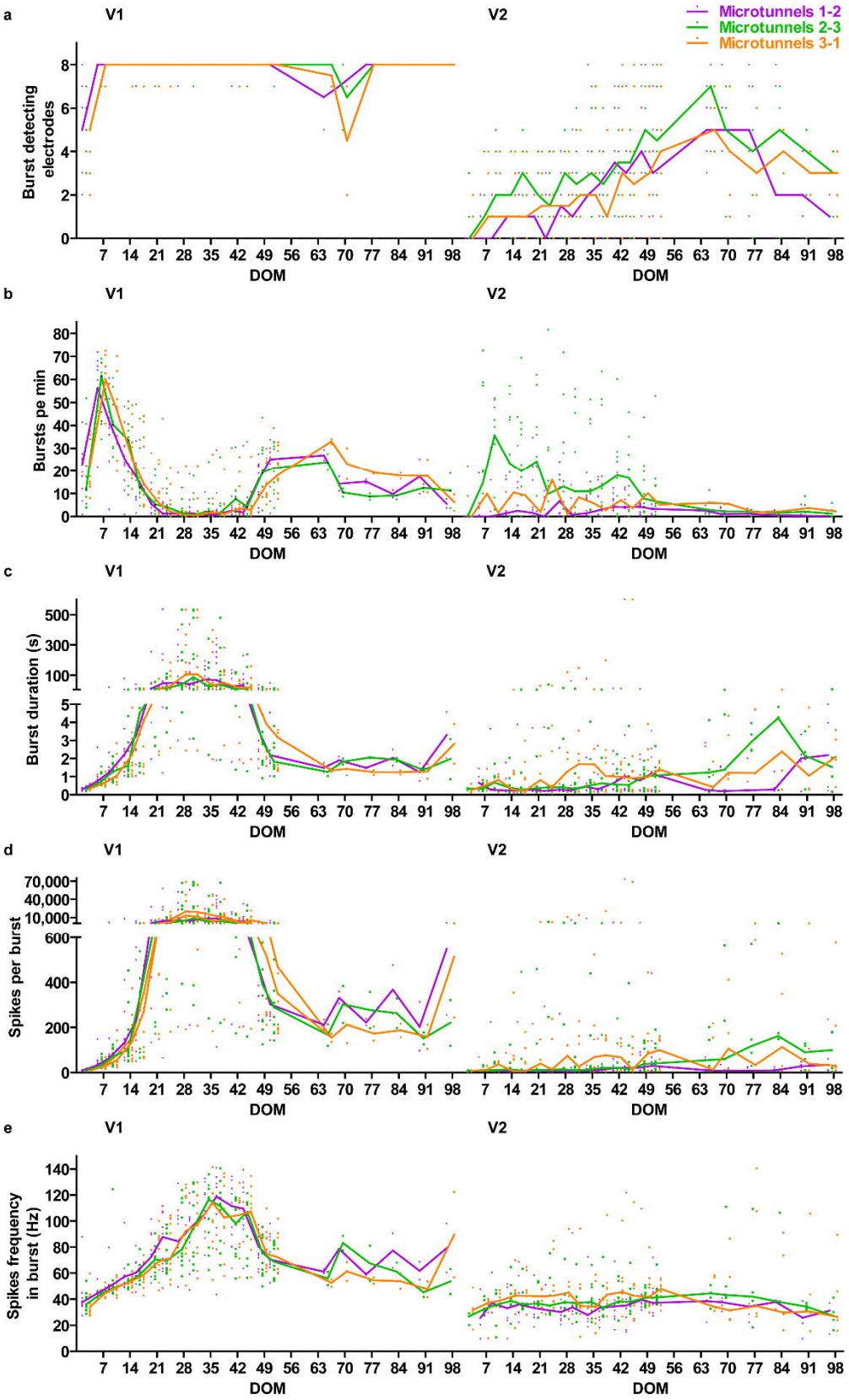

Supplementary figure 6 | Burst activity in microtunnel electrodes. The timeline for custom MEA version 1 (V1) is on the left and the timeline for custom MEA version 2 (V2) on the right in each subfigure. **a**, Number of burst detecting electrodes. **b**, Number of bursts per minute. **c**, Burst duration. **d**, Number of spikes per burst. **e**, Spike frequency in burst. Lines connect the group medians. DOM 3-52: n_{V1} = 11, n_{V2} = 10. DOM 66-98: n_{V1} = 2, n_{V2} = 5.

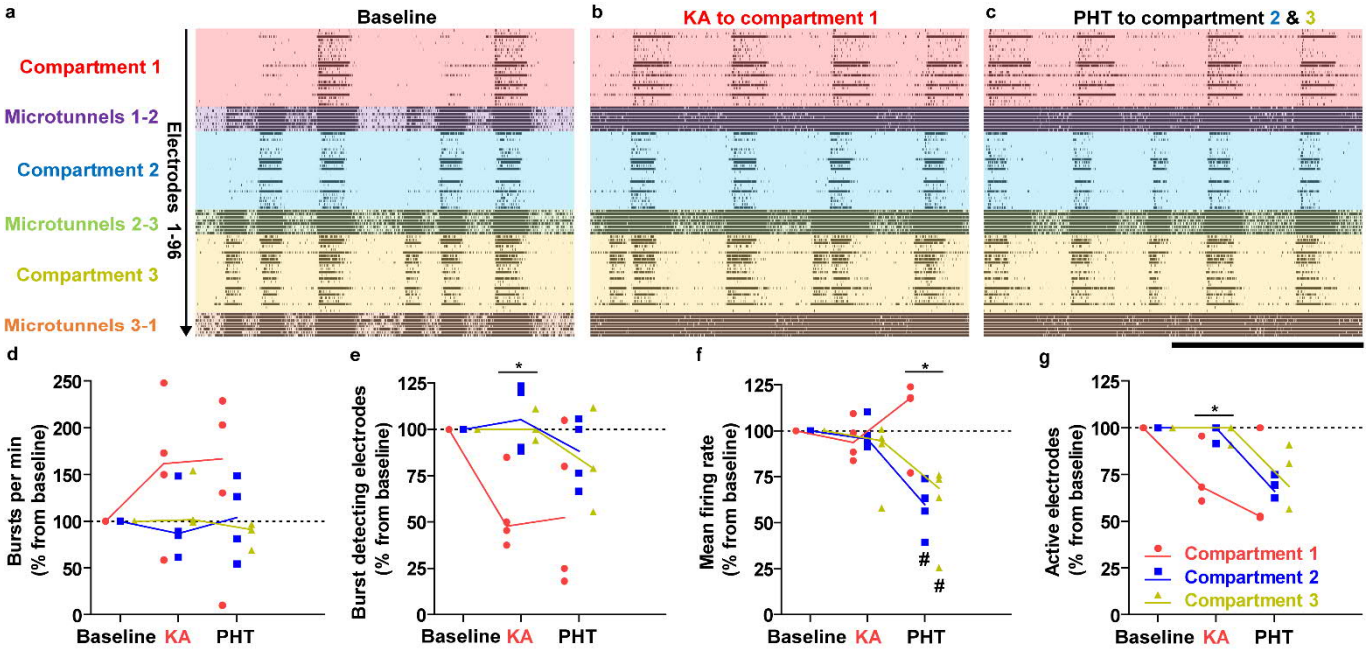

Supplementary figure 7 | Effect of kainic acid in compartment 1 and effect of phenytoin in compartments 2 and 3. **a**, Representative 1 min raster plot from the baseline recording. **b**, Representative 1 min raster plot after adding 5 µM kainic acid (KA) to compartment 1. **c**, Representative 1 min raster plot after adding 50 µM phenytoin (PHT) to compartments 2 and 3. The representative set was recorded on DOM 56. Scale bar is 30 s. **d**, Effects of the treatments on the number of bursts per minute in burst detecting electrodes. **e**, Effects of the treatments on the number of burst detecting electrodes. **f**, Effects of the treatments on mean firing rate in active electrodes. **g**, Effects of the treatments on number of active electrodes. The results in **d-g** are calculated as percent from baseline and the solid lines connect compartment medians. The effect of treatments in each compartment is analyzed with the Friedman test, and # stands for $p < 0.05$ in the Wilcoxon signed-rank *post hoc* test (with Bonferroni's corrections) against baseline. The difference between different compartments in each treatment is analyzed with Kruskall-Wallis test and * stands for $p < 0.05$. $n = 4$.